Chapter 17
Embedding Sensors in FDM Plastic Parts During Additive Manufacturing

Lexey R. Sbriglia, Andrew M. Baker, James M. Thompson, Robert V. Morgan, Adam J.Wachtor, and John D. Bernardin

Abstract In additive manufacturing, there is a necessity to qualify both the geometrical and material characteristics of the fabricated part, because both are being created simultaneously as the part is built up layer by layer. Increased availability of open source fused deposition modeling machines has expanded the parameter space for which the user has control during the build process. This work quantifies the effects of operator choices, such as print speed, printer head and build plate temperatures, layering thickness, or building in a thermally controlled or fully open environment, on the quality and reproducibility of the build. Modal analyses were performed on completed builds using an electrodynamic shaker and integrated circuit piezoelectric accelerometers embedded in the parts during the build process. Experimental measurements of the fused deposition modeled parts were benchmarked against eigenvalue analysis results for an idealized part with homogenous material properties to gauge the suitability of such analysis to fused deposition modeling additive manufacturing. Follow on work will use this embedded technique for state-of-health monitoring in deployed systems and real-time diagnostics and control of the build process.

Keywords Additive manufacturing • Fused deposition modeling • FDM • Modal analysis • Embedded sensors

Nomenclature

AM	Additive manufacturing
CAD	Computer-aided design
DAQ	Data acquisition
FDM	Fused deposition modeling
FEA	Finite element analysis
FFT	Fast fourier transform
SoH	State-of-health
STL	Stereolithography file
3D	Three dimensional

17.1 Introduction

Additive manufacturing (AM), more broadly know as three-dimensional (3D) printing, is the process by which an object is created vertically, layer-by-layer, in a Cartesian coordinate system. A variety of AM techniques have been developed for a wide range of printed materials, ranging from titanium and steel alloys [1] to cakes and gummy candies [2, 3]. The AM

L.R. Sbriglia
Department of Mechanical Engineering, University of Nevada, Reno, 1664 N. Virginia Street, Reno, NV 89557, USA

A.M. Baker
Materials Physics and Applications Division, Los Alamos National Laboratory, P.O. Box 1663, Los Alamos, NM 89557, USA

J.M. Thompson • R.V. Morgan • A.J. Wachtor (✉) • J.D. Bernardin
Applied Engineering and Technology Division, Los Alamos National Laboratory, P.O. Box 1663, Los Alamos, NM 87545, USA
e-mail: ajw@lanl.gov

M. Mains (ed.), *Topics in Modal Analysis & Testing, Volume 10*, Conference Proceedings of the Society for Experimental Mechanics Series, DOI 10.1007/978-3-319-30249-2_17

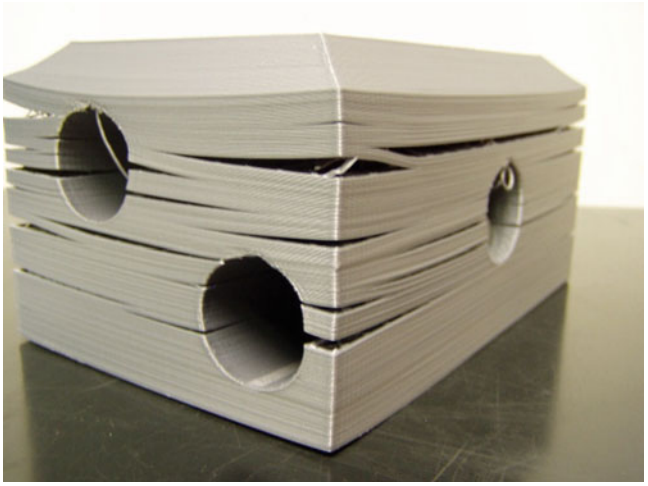

Fig. 17.1 Failed FDM part showing extensive delamination between printed layers

method used in this paper is known as fused deposition modeling (FDM). FDM is an AM technique commonly used for plastic parts which extrudes spooled thermoplastic material through a nozzle that heats the plastic to its melting point. The heated plastic is deposited in sequential two-dimensional layers to create the desired 3D object design [4]. Heat is transferred from the newly added plastic to the previous layer below it, partially re-melting that layer and bonding the layers together.

AM is advantageous because it can lower manufacturing costs of complex geometrical designs and reduce lead times [4], allows for rapid prototyping and design iteration, and can reduce the need for post processing [1]. A recent emergence of low cost, open source FDM printers have opened up the technology to a much larger user base. These open source printers give the user complete control of the wide array of print parameters, e.g. material, print head temperature, bed plate temperature, print speed, layer thickness, shell thickness, infill percentage, etc. However, putting the control into an inexperienced user's hands can result in a steep learning curve of identifying which parameters most greatly contribute to print failures, as in Fig. 17.1. Final geometrical and structural quality of parts is also most often determined by the individual's own success with a trial and error approach.

Material properties for AM parts are formed during the build process. Even with constant printer settings, the material properties can vary throughout the part depending on the part geometry, how much heat is retained in the previous layer when the next layer is printed, and how much heat is conducted from the print bed through the part. In this work, vibration analysis [5–7] was used as a means to quantify the effects operator choices for key parameters have on the structural characteristics of completed parts. Results are compared against a numerical solution of an eigenvalue analysis, for which constant material properties are assumed, to assess the extent to which these tools may be used to help gain insight into FDM produced parts.

There are a wide variety of applications for which embedding sensor technology directly into the part is desired to protect the sensor from harsh environments and prolong the lifetime of the sensor in use. In this work, sensors were embedded into the builds in order to directly measure the frequency response of the part during vibration testing. Although not necessary for this application, embedding the sensors did allow assessment of sensor embedment in FDM parts for future needs.

17.2 Experimental Setup

17.2.1 3D Printer

A Lulzbot Taz 5 with a 0.013 in. diameter extruder nozzle was used for printing all test articles. The print bed of the Taz 5 is 11.81 in. × 11.81 in. consisting of a borosilicate glass plate (0.118 in.) between a polyetherimide film print surface (<0.04 in.) and an adhesive silicone pad heater (0.118 in.). The gantry housing the print head translated in the x- and z-directions, while the print bed translated in the y-direction. Print parameters were set and G-code was generated using Cura Lulzbot Edition software.

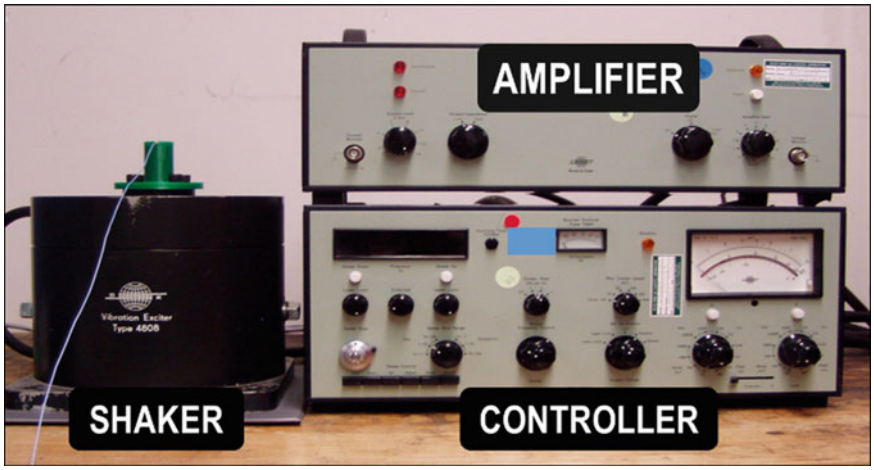

Fig. 17.2 Brüel & Kjær electrodynamic shaker setup

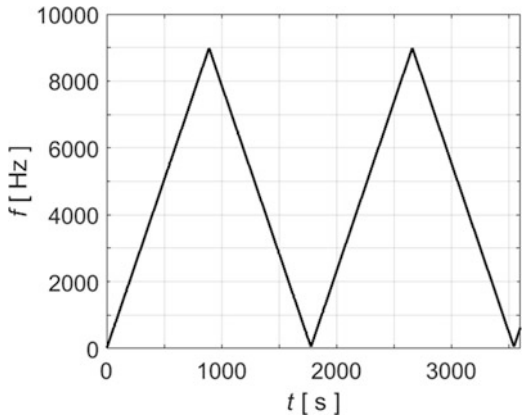

Fig. 17.3 Excitation frequency sweep performed for each printed part using Brüel & Kjær electrodynamic shaker

17.2.2 Shaker Table

Modal analysis was performed using a Brüel & Kjær shaker system consisting of the 4808 electrodynamic shaker, 2712 power amplifier, and 1047 exciter controller, pictured in Fig. 17.2. The table had a diameter of 2.45 in. and bare table operable frequency range of 5 to 10 kHz and maximum acceleration of 71 g. The controller was programmed to perform a repeated linear frequency sweep from 50 to 9 kHz and data was collected for each part for just over 4 complete sweeps as shown in Fig. 17.3. The data had very little variance (<0.5 % mean value) between sweeps for a given data collection run, so although all collected data is reported here, that from repeated sweeps for a given part are essentially indistinguishable from one another.

17.2.3 Data Acquisition

Frequency response measurements were collected using PCB Model 352A21 integrated circuit piezoelectric accelerometers powered with a 2.1 mA constant current supply from a National Instruments USB-4431 DAQ system with a sampling range from 1 to 102.4 kS/s with a resolution of 2.1 mS/s that was controlled using Matlab. The single axis accelerometers were specifically chosen for their compact design and measurement accuracy—0.02 oz weight, <0.02 $in.^3$ total volume, 10 mV/g sensitivity (±15 %), and ±500 g peak measurement range. An accelerometer was attached to the flat surface of one of the hex bolts used to anchor the part to the shaker table to measure the frequency at which the shaker was accelerating the part. The frequency response for the accelerometer on this bolt was measured directly against an accelerometer on the bare table and found to have average gain of 1.0804 with a standard deviation of 0.1316, which is orders of magnitude below the response level from the parts and therefore deemed acceptable for use as a measurement of the forced acceleration of

the table. The frequency response of the part was measured using a second accelerometer that was either embedded into the part during the build or place on the top surface of the column. In all cases, adhesion of the accelerometer to the part was performed using petro wax (PCB 080A109).

17.2.4 Part Design

A simple geometry of a single cylindrical column of 1 in. diameter (D) and 2.75 in. height (H) with solid infill was chosen for this study. To make for direct part mounting to the electrodynamic shaker used to perform the modal analysis, a flanged base (D: 3 in., H: 0.25 in.) was added to the cylindrical column that included four 5/16 in. holes corresponding to the bolt pattern on the Brüel & Kjær 4808 shaker described above. In order to embed the accelerometers directly into the build, a cavity based on the specific geometry of the PCB 352A21 was in inserted into the column 1.75 in. above the flange base, Fig. 17.4. To accomplish the sensor embedment, the G-code generated by Cura was modified to include a 2 min pause in the print at the layer height before the cavity was to begin being covered over. During that time, the printer bed was translated to its maximum y-position to provide easy access for manual insertion of the accelerometer. Presumably a smaller pause time could have been used, but the 2 min was found to be sufficient to ensure that enough care could be taken to guarantee that no part of the inserted sensor was sticking out above the current highest printed layer before printing resumed. In doing so, the tool path of the printer head was completely unobstructed for printing subsequent layers.

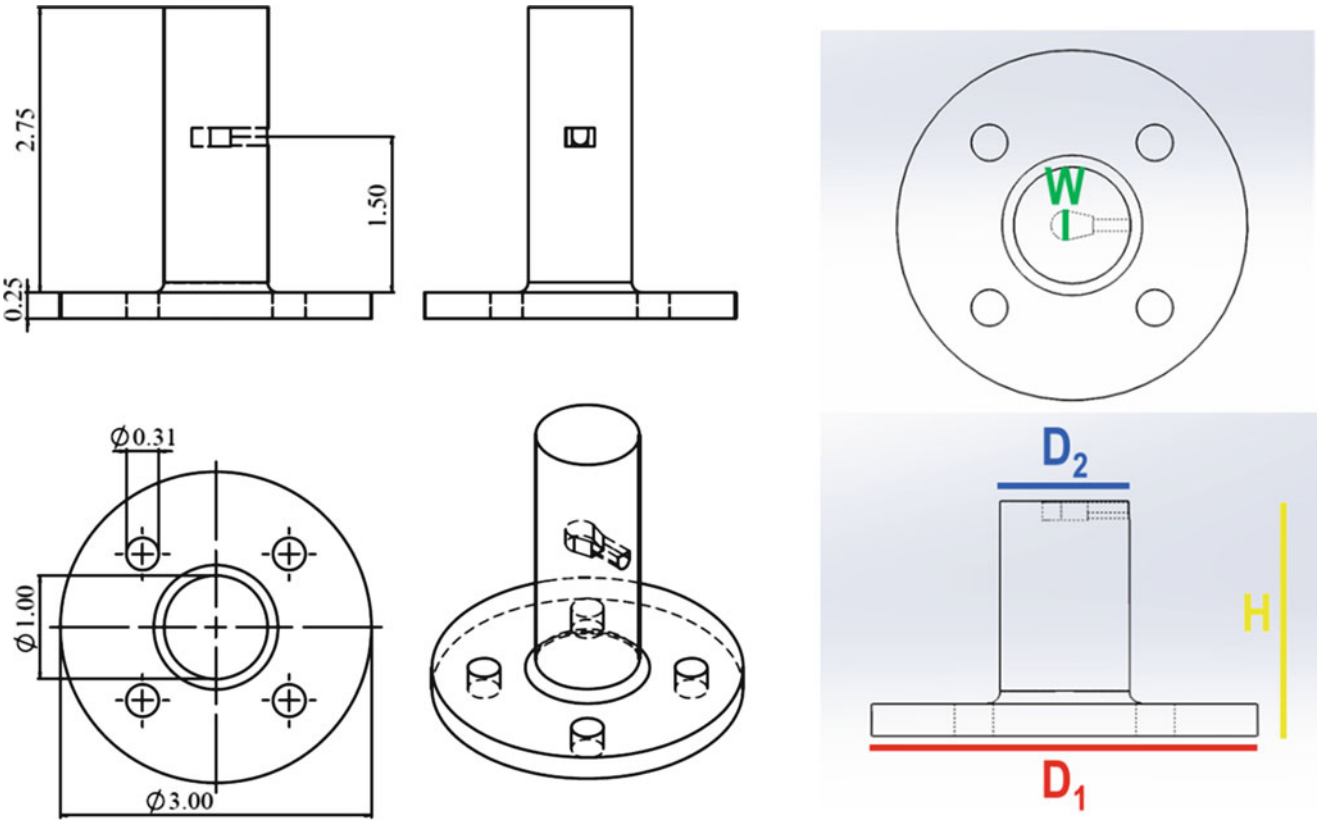

Fig. 17.4 Geometry of test articles with measurements shown in inches (*left*). Measurements used for geometrical quantification of material choice (*right*)

17.3 Results

17.3.1 Material Choice

The Lulzbot is capable of printing with a variety of stock materials; high impact polystyrene (HIPS), acrylonitrile butadiene styrene (ABS), and polylactic acid (PLA) were all assessed to be used in this study. To do so, parts were printed with each material up to the layer before the cavity was to be covered using the manufacturer's recommended settings, Fig. 17.5. The printed parts were then measured to see how closely they compared to the computer-aided design (CAD) geometry, Table 17.1.

As seen in Fig. 17.5, both the ABS and HIPS parts produced very poor surface finishes and each layer within the column had a larger footprint than was prescribed in the CAD design. This resulted in the sensor cavity being too small to fit the accelerometer. Since it was desired to have as short of a pause in the print as possible to embed the sensor, so that chances of delamination were minimized, this aspect of the print was highly undesirable.

Although, the CAD file could have been adjusted to accommodate for the increased footprint with ABS and HIPS, it was found that the PLA was able to provide a much better quality part that had better surface finish and could house the accelerometer without any CAD modification. Therefore, PLA offered the best option for successful prints when changing only a single parameter from the recommended setting and was chosen to be used for all subsequent prints, the parameters of which are listed in Table 17.2.

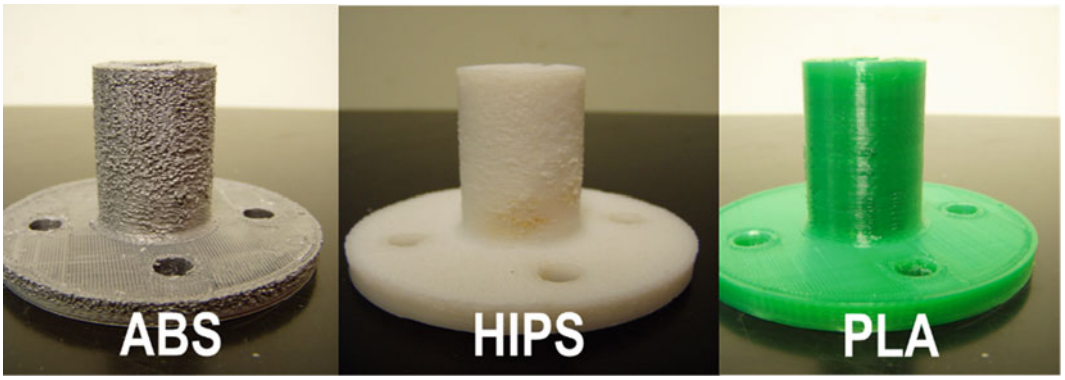

Fig. 17.5 Parts printed up to the top of the accelerometer cavity with manufacturer's suggested settings for different materials

Table 17.1 Measurements of variation from CAD geometry for key geometrical dimensions of parts printed only up to the top of the sensor cavity, see Fig. 17.4

Material	D_1 (in)	D_2 (in)	W (in)	H (in)
ABS	(−) 9.1e-3	(+) 0.04	(−) 3.9e-3	(+) 0.02
HIPS	(−) 0.01	(+) 0.02	(−) 7.1e-3	(+) 0.02
PLA	(−) 7.1e-3	(−) 7.1e-3	(+) 0.01	(+) 0.02

Table 17.2 Print parameters for each build

Build #	1-3	4	5	6	7	8	9	10
Layer height (in)	9.45e-3	9.45e-3	**0.019**	**4.72e-3**	9.45e-3	9.45e-3	9.45e-3	9.45e-3
Shell thickness (in)	0.059	0.059	0.059	0.059	0.059	0.059	**0.256**	**0.512**
Bottom/Top thickness (in)	0.031	0.031	0.031	0.031	0.031	0.031	0.031	0.031
Fill density (%)	100	100	100	100	100	100	100	100
Print speed (in/s)	1.97	1.97	1.97	1.97	**2.95**	**0.984**	1.97	1.97
Printing temperature (°F)	401	401	401	401	401	401	401	401
Bed temperature (°F)	140	140	140	140	140	140	140	140
Filament diameter (in)	0.114	0.114	0.114	0.114	0.114	0.114	0.114	0.114
Filament flow (%)	100	100	100	100	100	100	100	100
Embedded sensor	Y	**N**	**N**	**N**	**N**	**N**	**N**	**N**
Estimated print time (h)	4.60	4.60	**2.48**	**8.92**	**3.60**	**7.67**	**5.32**	**5.73**

Differences from prints done with recommended setting highlighted in bold

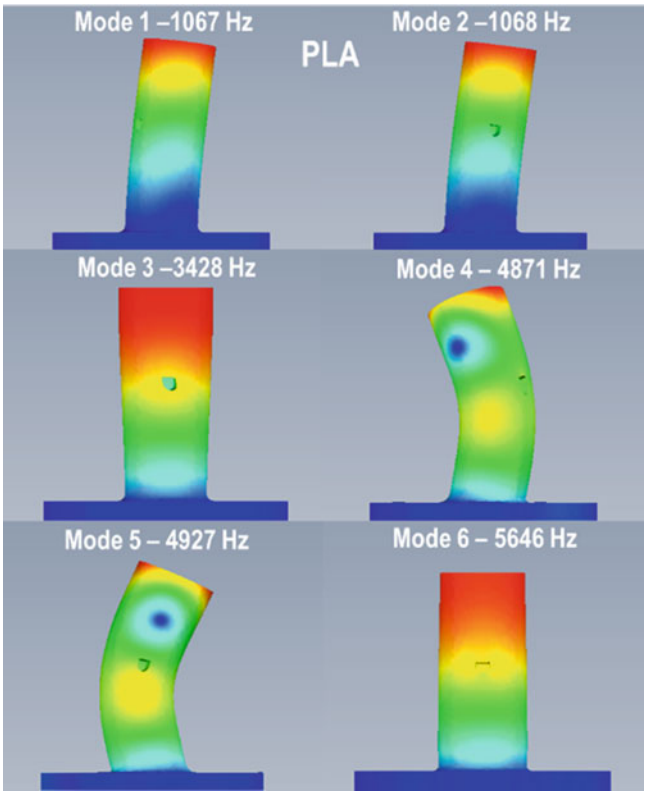

Fig. 17.6 Mode shapes for modes 1-6 determined from Solidworks Simulation frequency analysis of PLA part

Table 17.3 First 8 modes resulting from the Solidworks Simulation frequency analysis for the PLA test article

Mode #	1	2	3	4	5	6	7	8
f (Hz)	1067	1068	3428	4875	4928	5646	9847	9888
MP_x (%)	35.5	–	–	18.3	–	2.3e-2	16.5	–
MP_y (%)	1.1e-3	35.6	1.1e-3	–	18.5	–	–	15.5
MP_z (%)	–	–	–	3.8e-2	–	47.3	5.3e-3	–

Mass participation (MP) for each Cartesian direction is listed, but values that fell below 0.001 % were negligible and therefore omitted from the table

17.3.2 Frequency Analysis Simulation

A Solidworks Simulation frequency analysis was performed using the CAD file for the test article. Restricted movement of the bolt holes and the portion of the bottom of the part that was in contact with the table was accounted for. Figure 17.6 shows the first six natural frequency modes that the eigenvalue analysis determined. Motion in the x- and y-directions was largely identical, with only a small frequency shift due to the presence of the asymmetric cavity introduced into the column to house the accelerometer. The mode pairs of 1-2, 4-5, 7-8 were largely characteristic of fixed-free beam motion, while mode three was a low energy torsional mode. Table 17.3 shows that the mode with the greatest mass participation (MP) was mode 6, which is a compressional mode in the z-direction. The shaker was set up to accelerate the test articles in the z-direction, therefore, large amplifications of this mode were expected to be seen in the experimental measurements.

17.3.3 Reproducibility Between Builds with Identical Settings

A set of four prints was performed with identical settings to assess the amount of variation that can be attributed simply due to the build process. Embedded sensors were placed in three of the four prints. This operation was done manually. After

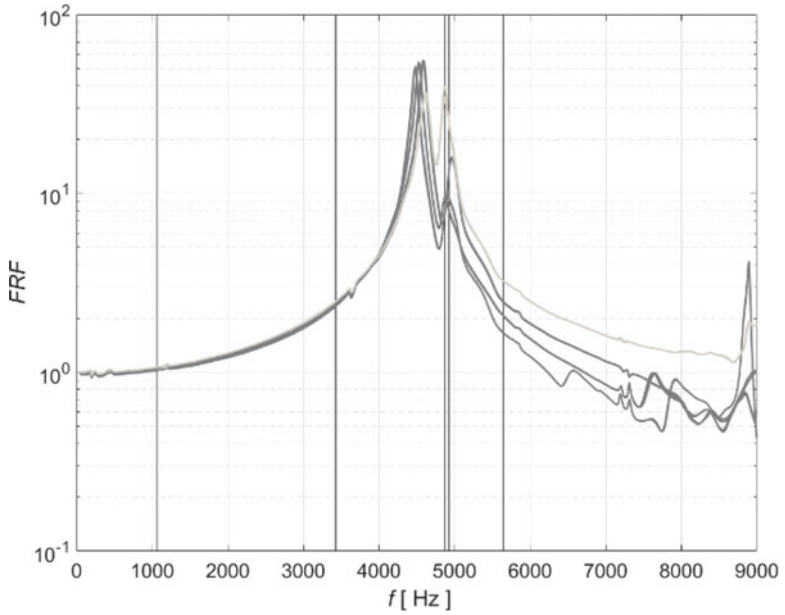

Fig. 17.7 Frequency response function for Build # 1-3 (*dark gray*) and 4 (*light gray*). Vertical lines at resonant frequencies predicted by Solidworks Simulation

completing the task once, it was found that the 2 min pause programmed into the G-code was sufficient to place the sensor and ensure that it would not interfere with the path of the printer head when printing resumed. The pause duration could have been reduced to around 30 s, but desire to keep consistency between these prints was higher than the small time savings that would have provided. In fact, the same 2 min pause was incorporated into the G-code for all prints, regardless of whether an accelerometer was placed in the print, or mounted to the top of the print after completion.

Since the sensors used for measurement were only single axis accelerometers aligned to measure in the z-direction, measured frequency response amplitudes were expected to be greatest around the frequencies associated with either modes with large z-motion or containing some component of motion in the z-direction. In Fig. 17.7, the average peak in the frequency response function (FRF) was found at 4553 Hz with a standard deviation of 63 Hz for these prints. Low frequency response is largely governed by the material stiffness. In this region, excellent agreement was observed between all the FRF curves below the peak value, including a small bump in the FRF around 1200 Hz and a dip at 3630 Hz, which were likely due to contributions from modes 1–3. The maximum peak and secondary peaks are believed to be associated with modes 4–6. Although, there is some rough agreement with the values of the resonant frequencies measured in the experiments and those predicted by the Solidworks Simulation frequency analysis that helped with this interpretation, the actual prediction of the resonant frequencies was well off of that measured. This may be attributed to the fact that the Solidworks Simulation assumed that the part is 100 % solid and has constant material properties. However, that is not the case for these FDM parts.

17.3.4 Effect of Print Layer Height

To assess the effect of print layer height, the layer height was doubled (Build # 5) and halved (Build # 6) from that prescribed for Builds # 1-4. Doubling the layer height resulted in a very poor surface finish and a significant shift in the peak FRF down to 4295 Hz, Fig. 17.8. When the layer height is increased in FDM, the amount of surface contact between the recent layer and the previous layer is reduced, weakening the fusion between those layers. Thus, this downwards shift is most likely due to the stiffness of the part being reduced as the adjoining layers were not fully fused throughout the build.

Halving the layer height did have the opposite effect of doubling it, in that the max FRF peak shifted upwards to 4643 Hz, just outside the range seen in Build # 1-4. The fact that this shift was smaller than that seen for doubling the layer height may be attributed to the fact that the settings for Build # 1-4 likely already had adequate layer fusion, so there was not much more opportunity left to increase the surface contact between the layers. Although, Build # 6 did have the best surface finish and its shift in the peak FRF frequency suggests it has increased strength, the time required to build the part was nearly 9 h. In that time nearly two full parts would have been capable of being printed using the basic printer settings of Build # 1-4.

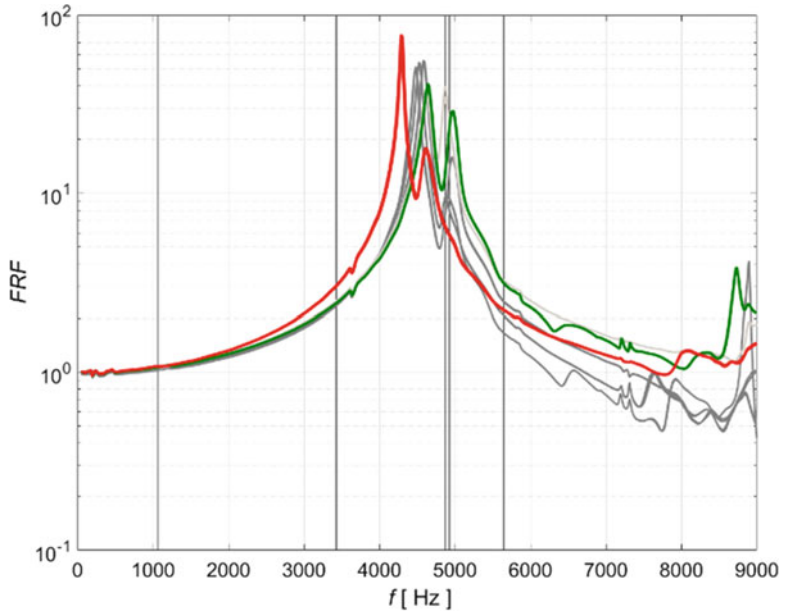

Fig. 17.8 Frequency response function for Build # 1-3 (*dark gray*), 4 (*light gray*), 5 (*red*), and 6 (*green*). Vertical lines at resonant frequencies predicted by Solidworks Simulation

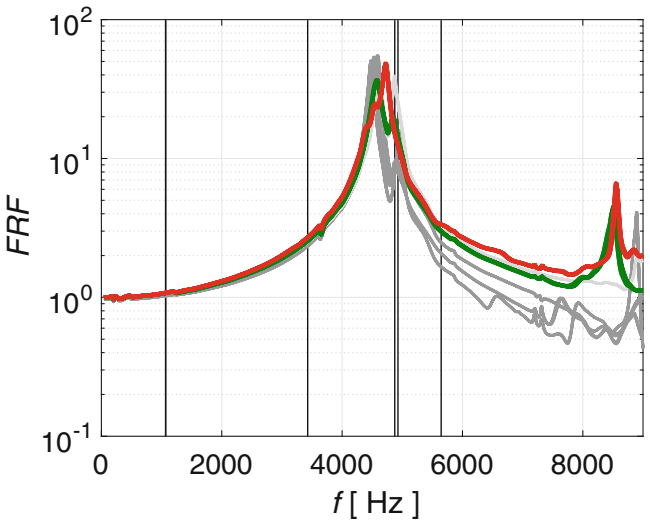

Fig. 17.9 Frequency response function for Build # 1-3 (*dark gray*), 4 (*light gray*), 7 (*red*), and 8 (*green*). Vertical lines at resonant frequencies predicted by Solidworks Simulation

17.3.5 Effect of Print Speed

Often the operator of an FDM machine is faced with a tradeoff between print resolution and the time to print completion. In this work the print speed was tested by increasing the speed 1.5x and decreasing it 0.5x. The increased speed resulted in a build with lower quality surface finish, and moved the primary FRF peak up to 4726 Hz, Fig. 17.9. There was also a small bump in the FRF around 4550 Hz, that may correspond to the same primary mode that was found in Build #1-4. For the build carried out at the slower speed, the FRF peak was 4581 Hz and the build quality was comparable to Build # 1-4. Therefore, this option did not produce any advantages over the basic print settings. And if a longer time is available to complete the print, one should instead consider reducing the layer height instead of the print speed to improve surface finish of the completed part.

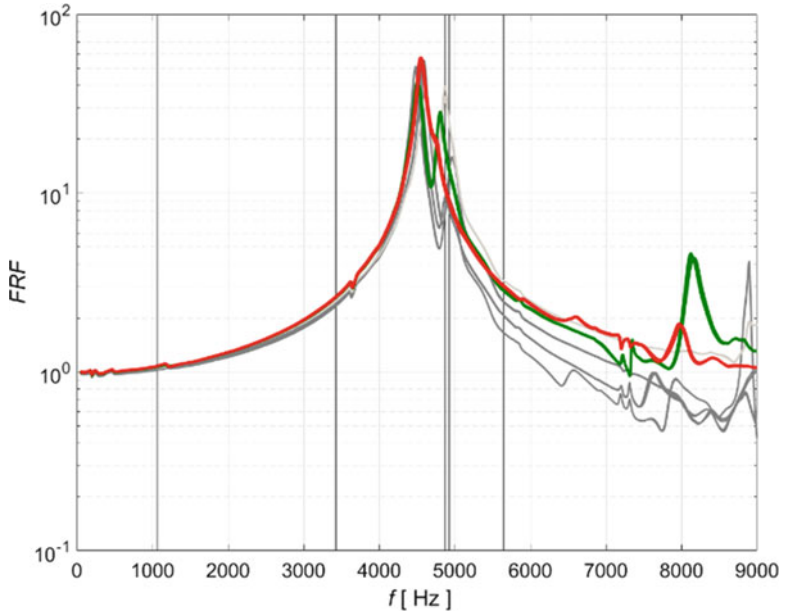

Fig. 17.10 Frequency response function for Build # 1-3 (*dark gray*), 4 (*light gray*), 9 (*red*), and 10 (*green*). Vertical lines at resonant frequencies predicted by Solidworks Simulation

In both Build # 7 and 8, a distinct peak in the FRF was measured around 8600 Hz. A peak of this magnitude was not seen in Build # 1-4 or in the Solidworks predictions. This may be a result of the Young's modulus differing between these FDM builds and the values given in the literature that were used in the Solidworks simulation. The inhomogeneities in the FDM parts appear to reduce the stiffness of the part significantly enough that Modes 7-8 then fell into the measurement range.

17.3.6 Effect of Tool Path

The tool path prescribed by Cura Lulzbot Edition first printed the outside perimeter of the cylinder in circular paths until the shell thickness was met, then performed the solid infill largely using a linear snake pattern. By increasing the shell thickness, more circular print paths were used in the build. The shell thickness was adjusted to half the cylinder radius and to the full radius. Figure 17.10 shows the effects that these changes have on the frequency response. Build # 9 consisted of a column with a radius of half axisymentric and half linear tool paths, and although the peak in the FRF was 4514 Hz and close to that of Build # 1-4, the secondary peak was moved in so close to the primary peak that it almost was nearly indistinguishable from the decay from the primary resonance peak. The build with a fully circular build path also had a primary peak, 4558 Hz, that was close to those of Build # 1-4, and a secondary peak that was shifted down. However, in Build # 10 the secondary is still clearly distinguishable from the primary peak.

In both Build # 9 and 10, a prominent high frequency peak is present around 8000–8200 Hz. Similar to the results from changing printer speed, this suggests that this printing change resulted in fundamentally different structural properties than those built using the manufacturer's recommended settings and is a demonstration that the tool path used to build the part also affects its material properties. On one hand, this results should not be surprising, because the tool path defines the thermal history of the part. However, controlling the tool path is largely outside of the user's hands, as it is an automated process done through software, putting a limit on the extent to which the user's choices can control the build.

17.4 Conclusion

This work largely lays the foundation for a much larger parameterized study of operator choices for FDM builds using open source machines, and also future work for embedding sensors into AM parts. Due to the limited amount of information collected using single axis accelerometers, the orientation of excitement relative to the part was later modified to excite a

greater response of the fixed-free beam modes. This was accomplished by fixing a 6061-T6 aluminum cube to the shaker and mounting the parts to the side of the aluminum fixture. The FRFs for the FDM parts using this orientation produced clear resonance peaks near, but almost always below, the predicted Solidworks Simulation predictions, suggesting that the effective stiffness of the FDM parts is lower than that which would be found in parts made through subtractive manufacturing of the same material. It is the intention of the authors to publish the results using the alternative excitation orientation in a future publication, but any interested reader is encouraged to contact the authors directly.

It was found that operator choices have a direct impact on the structural properties of the part, e.g. stiffness, and can be measured using techniques like the vibration analysis demonstrated here. The limited parameter variation presented suggests that there is a range for each of the values tested which result in a small variance from characteristics of the recommended printer settings. However, once outside that range, printer settings may result in significant deviations from what would have been measured with the recommended settings, e.g. doubling the print speed. A more detailed parameter variation should be performed to find these limits.

Analysis of a complete parameterized study could be used to guide operator choices and avoid user induced failure. As the tool path for the print was found to affect the thermal history of the print, and subsequently the material properties, the extent to which fine control over the material properties can be achieved is still an open question. If one were truly seeking to print an FDM part with homogeneous material properties, they would either need to simulate the thermal history of the build process and create an algorithm that adjusts the printer properties throughout the build, or be able to actively measure temperature in the top build layers and design a closed feedback control to be used during the print process.

Embedding sensors in FDM parts can be useful for state-of-health (SoH) monitoring in deployed systems [8]. The embedment method used in this paper was rather simple, so that parts could later be cut open and sensors removed for use in future studies. However, since this would not be desirable for SoH applications, the method may be improved upon to ensure that the sensor remains in proper contact with the part for its lifetime.

Acknowledgements The authors would like to thank the National Nuclear Security Administration's Minority Serving Institution Internship Program. Los Alamos National Laboratory (LANL) is operated by the Los Alamos National Security, LLC for the U.S. Department of Energy NNSA under Contract No. DE-AC52-06NA25396.

References

1. Wong, K.V., Hernandez, A.: A review of additive manufacturing. Int. Scholarly Res. Netw. Mech. Eng. **2012**, 1–10 (2012)
2. http://3dprintingindustry.com/food/
3. http://3dprinting.com/food/
4. Li, H., Taylor, G., Bheemreddy, V., Iyibilgin, O., Leu, M., Chandrashekhara, K.: Modeling and characterization of fused deposition modeling tooling for vacuum assisted resin transfer molding process. Additi. Manuf. **7**, 64–72 (2015)
5. White, C., Li, H.C.H., Whittingham, B., Herzberg, I., Mouritz, A.P.: Damage detection in repairs using frequency response techniques. Comp. Struct. **87**(2), 175–181 (2009)
6. Martínez, J., Diéquez, J.L., Ares, E., Pereira, A., Hernández, P., Pérez, J.A.: Comparative between FEM models and FDM parts and their approach to a real mechanical behavior. Proc. Eng. **63**, 878–884 (2013)
7. Chaitanya, S.K., Reddy, K.M., Harsha, S.N.S.H.: Vibration properties of 3D printed/rapid prototype parts. Int. J. Innov. Res. Sci. Eng. Technol. **4**(6), 4602–4608 (2015)
8. Stark, B., Stevenson, B., Stow-Parker, K., Chen, Y.Q.: Embedded sensors for health monitoring of 3D printed unmanned aerial systems. In: 2014 International Conference on Unmanned Aircraft Systems, 175–180, 2014